

Identification of large amplitude wind-induced vibration of ice-accreted transmission line based on field observed data

C.B. Gurung^a, H. Yamaguchi^a and T. Yukino^b

^a *Department of Civil and Environmental Engineering, Saitama University,
255 Shimo-Ohkubo, Saitama, 338-8570, Japan*

^a *Technical Research Center, Kansai Electric Power Co. Inc., Amagasaki, Japan*

Corresponding author: Professor Hiroki Yamaguchi
Department of Civil and Environmental Engineering
Saitama University
255 Shimo-Ohkubo, Urawa, Saitama 338-8570, Japan

Phone: 81-48-858-3552

Fax: 81-48-858-3552

Email: hiroki@post.saitama-u.ac.jp

Abstract

This study presents a method to identify the periodic galloping response and random gust response of transmission line based on field observed data and to separate major galloping component from mix mode of gust and galloping vibration. Time-averaged characteristics of wind-induced vibration are discussed based on spectral analysis and non-stationary characteristics are considered to identify the wind-induced vibration quantitatively by applying Prony's method in piecewise fashion. By applying highpass filter major galloping response component is separated from mixed response and characteristics of thus separated major galloping response component are compared with those of total response. Results of these analyses show possibilities of large amplitude galloping as well as gust response in in-plane vertical motion in ice-accreted transmission line. Applicability of random decrement method to estimate the existence of periodic correlated galloping component is also discussed.

Keywords

Transmission line; Field data; Galloping; Gust response; Identification; Prony's method; Filtering technique; Random decrement method

|

Introduction

Large amplitude wind-induced vibration of ice-accreted transmission line is frequently observed. Galloping, which is low frequency and large amplitude wind-induced vibration of ice-accreted transmission line, usually in moderately strong and steady wind is well recognized as one of the major wind-induced vibrations to cause failure. But it is realized that galloping is a rare and an unpredictable event caused by interaction of wind and ice accretion in conductor/s. If either ice or wind is absent, galloping cannot occur but even if both are present, galloping doesn't always result [1]. It is frequently reported that the amplitude of galloping of ice accreted transmission line could be very large, sometimes in the order of the sag of the line offering possibility of short circuiting among different phases [2-4]. On accounts of its possible damage due to possible flash over among phases and overloading of tower's arms, galloping of ice-accreted transmission line is major concern to the people in the field of Power Industry.

Galloping is one of the classical problems in overhead transmission lines in some climatic conditions, which has been studied by many researchers through field observations [5,6], wind-tunnel experiments [3, 7] and numerical analyses [8-10]. In spite of such numerous studies on galloping for several years, a practical protection method that is recognized as fully reliable has not been developed [2]. Minimization or control method of galloping of transmission lines still depends on field trial and error procedure [10]. In order to develop an effective method of controlling or minimizing galloping, it is indispensable to understand its characteristics such as characteristics of galloping orbit, frequency, amplitude, negative damping and mode of vibration. However, timely change in configuration of cross-section of transmission line, which causes changes not only in aerodynamic characteristics but also in natural dynamic characteristics as for example change in torsional frequency in relation to translational frequencies, brings further uncertainties in the understanding of characteristics of galloping [11]. In order to characterize galloping of large bundle transmission line configuration, Kansai Electric Power Company (KEPCO), Japan has been observing and analyzing any large amplitude wind-induced vibration of Tsuruga Test Line in the presence of wind and ice, and galloping observed in the test line have been reported as vertical, inclined and horizontal galloping [5]. However, attempt has not been made to identify whether the events are really driven by instability mechanism i.e. due to negative aerodynamic damping. On account of high flexibility of transmission line, large amplitude random vibration due to atmospheric gusty wind cannot be overlooked. Based on numerical analysis, the possibility of large amplitude random gust response has been pointed out in turbulent wind [10].

For the rational design of transmission line and smooth operation, control or minimization of both gust response and galloping vibration is indispensable. Since characteristics of galloping and gust response are entirely different, the way to minimize or control them would be different. It is, therefore, necessary to identify galloping and gust response even though the order of amplitude for both categories of wind-induced vibration are of same order. Identification of amplitude, frequency, damping ratio, mode of vibration and characteristics of oscillation envelopes are necessary for the characterization of a vibration. Generalization of characteristics of galloping observed in nature, however, must include a large number of observations which can represent

wide ranges of metrological conditions of ice and wind and it is necessary to develop a standard method of identification to analyze a large number of field data.

In this study, a method of data analysis is proposed to identify large amplitude wind-induced vibration of ice-accreted transmission line based on data observed in Tsuruga Test Line by KEPCO. The method starts from spectral analysis to discuss the time-averaged characteristics of wind-induced vibration. Prony's method is then introduced in piecewise fashion to identify the dominant harmonic component which can represent the major galloping component in a response. Followed by the results of spectral and Prony's analyses, filtering technique is employed to separate the major gust and galloping components of response in a vibration that consists of significant amount of gust and galloping response. Applicability of random decrement method is also discussed to estimate galloping component in a response by eliminating random response component.

Outline of transmission line and field measurement

The study is based on field-measured data of wind-induced vibrations of ice accreted Tsuruga Test Line observed by KEPCO in 1996 and 1997. Tsuruga Test Line is located near Tsuruga Bay, a place with one of the typically severe climatic conditions in winter favoring galloping of overhead transmission line. There are three phases of Tsuruga Test Line namely Phase A, Phase B and Phase C, while only events in Phase B and Phase C are considered in this study. Phase B and Phase C are 4-bundled conductor with two semi-suspension spans and 6-bundled conductor with dead-end span lines, respectively. Fig. 1 shows top view of Phase B and Phase C in Tsuruga Test Line (Phase C comprises of a span with 8-bundled conductor but only events observed in the span with 6-bundled conductor are discussed). The detail geometrical and dynamic descriptions of Tsuruga Test Line are listed in Tables 1 and 2, respectively. Mode of vibration in Table 2 is expressed in terms of number of loops in a span. It is to be noted that frequency of quasi-one loop vertical mode is higher than two loop vertical mode in case of Phase C as shown in Table 2. It is due to the fact that quasi-one loop vertical mode in dead-end span requires higher dynamic tension head than in two loops vertical mode [4]. On account of possible global tension coupling in between two spans through suspension support, however, it is not the case in Phase B.

Video pictures of targeted lamp placed at each quarter span and mid span of the transmission line were taken by optical gyroscope and their movement was recorded in sampling period of 0.2 seconds and 0.1 seconds for the events observed in year 1996 and 1997, respectively. It should be noted that some interruptions in the measurement by the video recording are seen in the data clearly for different instances of measurements on account of bad weather (bad light/vision). Wind velocity was also measured at the time of vibration at the central tower of the test line.

Typical wind-induced vibration of ice-accreted Tsuruga Test Line

Several wind-induced vibration events of ice accreted Tsuruga Test Line were observed in Phase B and Phase C. From the records of vertical and horizontal responses,

oscillation envelopes are drawn and thus drawn Lissajous diagrams are used to characterize the large amplitude vibration of ice-accreted transmission line as usual [5]. Observation on the time series of responses and the Lissajous diagrams revealed wide varieties of wind-induced vibrations. Based on the orientation and the steadiness of the Lissajous diagrams, all observed events could be divided into three typical categories, namely Events 1, 2 and 3. Events 1 and 2 are the vibrations observed in phase C (6-bundled conductor, dead-end span) in 1997 and 1996, respectively, and Event 3 is the vibration observed in Phase B (4-bundled conductor, semi-suspension span) in 1996. Furthermore, Events 2 and 3 were observed at the same instant with the same wind condition and Event 1 was observed at different instant during different wind condition. Lissajous diagrams of each representative event at quarter span and mid span are depicted in Fig. 2.

The Lissajous diagram of Event 1 at quarter span is oriented almost vertical and path of oscillation is relatively steady, while very small fluctuating response component can be seen at mid span as shown in Fig. 2 (a). On the contrary, the Lissajous diagrams of Events 2 and 3 at both quarter span and mid span are oriented obliquely at an angle of $30 \sim 45$ degrees with unsteady path of oscillation as shown in Figs. 2 (b) and (c). A careful observation of the Lissajous diagram of Event 2 at quarter span reveals that the oscillation is principally vertical but drifted obliquely. The corresponding time series of vertical response in these representative events at quarter span are depicted in Fig. 3 along with the time series of wind velocities measured at Tower No. 2 (Fig. 1). As is seen from Fig. 3, the vertical response of Event 1 is relatively stationary in agreement with the wind velocity as compared to those of Events 2 and 3 which have higher fluctuation reflecting higher mean wind velocity with large fluctuation.

It can be understood from Fig. 2 that the peak-to-peak amplitude in vertical motion in each event is almost two meters, while large variation can be seen in horizontal peak-to-peak amplitude, ranging from about one meter to four meters. Since all the observed vibrations are associated with large amplitude and with relatively longer period, there is a possibility of interpreting those events as galloping. Accordingly, Event 1 could be interpreted as vertical galloping and Events 2 and 3 as oblique galloping. Such interpretations, however, could be misleading without considering whether the vibration has negative aerodynamic damping or not. Further analyses have to be performed in order to identify galloping with negative aerodynamic damping and random vibration due to gusty wind.

Identification of observed wind-induced vibration

Methods of identifying different categories of wind-induced vibrations of ice-accreted transmission line based on the field observed records are discussed in this section. Qualitative identification of wind-induced vibrations is first discussed based on time-averaged characteristics of responses and wind velocities by spectral analysis. Time dependent analysis based on Prony's method is then applied for quantitative discussion on amplitude, frequency and damping ratio of major galloping component.

Spectral analysis for time averaged characteristics of response

Spectral analysis is carried out to investigate the time-averaged characteristics of

wind-induced responses and wind velocities in frequency domain.

The power spectrum diagrams of Events 1, 2 and 3 at quarter span are shown in Fig. 4. A clear peak at the frequency close to the natural frequency of the in-plane two-loops mode can be seen in the power spectra of vertical response in Events 1 and 2 as shown in Figs. 4 (a) and (b). This peak frequency is well separated from the frequency of wind turbulence as depicted in Fig. 5 where the power spectra of wind velocities are given. It reveals that the response component corresponding to the peak frequency cannot be the result of forced vibration due to wind turbulence.

Very large contribution of low frequency response component is evident in Events 2 and 3, as shown in Figs. 4 (b) and (c). The frequency of this component is very low without any possibility of dynamic amplification due to resonance. The power spectrum of wind velocity during the Events 2 and 3, depicted in Fig. 5 (b), shows that most of the energy of wind fluctuation is associated with low frequency component in agreement with observed response component in the low frequency. This response component can be, therefore, treated as a quasi-static response induced by the slowly varying wind velocity. With wind tunnel experiment on scaled model of transmission line, it has also been pointed out that the quasi-static response, called as background response, is the biggest contributor to total forced vibration response [7].

This kind of quasi-static response can be significant in and peculiar to transmission line structures because of their high flexibility. The quasi-static response component in Event 3 is, for example, more significant than in Event 2, while Events 2 and 3 were observed under the same wind condition. This is due to the fact that the structure of Phase B (semi-suspension span) in which Event 3 was observed is more flexible than that of Phase C (dead-end span) in which Event 2 was observed. Another factor which affects on the significance of quasi-static response is, of course, the turbulence intensity of wind. In fact, there exists significantly high energy of low frequency wind fluctuation in Event 2 than in Event 1, as shown in Figs. 5 (a) and (b), the quasi-static response in Event 2 is relatively larger than in Event 1 as shown in Figs. 4 (a) and (b).

Excluding the quasi-static response component, the power spectra of Event 3 at quarter span show the existence of numbers of peaks clustered together in narrow frequency band close to the natural frequencies of the in-plane and out-of-plane single-loop per span modes as shown in Fig. 4 (c). Same nature of power spectrum of horizontal response in Event 2 is observed. Because the power spectrum of wind velocity during Events 2 and 3, shown in Fig. 5 (b), contains a trace of wind turbulence with the frequency in the region of the one-loop natural frequency, the peaks in the power spectra of responses can be identified as the dynamic magnification due to resonance.

Filtering technique for exclusion of the quasi-static response

Based on the time-averaged characteristics of responses, typical wind-induced vibrations can be separated into the low frequency quasi-static component and the higher frequency component. The quasi-static component has a frequency well below the first natural frequency of transmission line, which can be well identified as gust response with confidence. According to characteristics of galloping, it can be said that such a low frequency quasi-static component never includes galloping component. Thus, for the purpose of identifying large amplitude wind-induced vibration as galloping, the

quasi-static component is out of concern and can be separated from the total response for further analysis. In order to exclude the quasi-static component, the highpass filter with cut-off frequency of 0.05 Hz is employed for Events 2 and 3.

The higher frequency component can contain random gust response due to wind turbulence and galloping or either of them. In order to identify whether the higher frequency component consists of gust response or galloping response or combination of them, it is essential to carry out further analysis which can take into account of time dependent characteristics of records.

Prony's method for identification of amplitude, frequency and damping ratio

Prony's method is applied to find out a dominant harmonic component in the higher frequency component of observed wind-induced vibrations. Since characteristics of galloping component can be changed with time, Prony's method was applied in piecewise fashion with respect to time in this study.

Applying Prony's method to a piece of time series of response, $x(t)$, weighted linear combination of exponential functions is considered as its model:

$$\hat{x}(t) = \sum_{i=1}^n B_i e^{\lambda_i t} \quad (1)$$

where $\hat{x}(t)$ is an estimated response by Prony's method, B_i is the i^{th} weighing factor and $e^{\lambda_i t}$ is the i^{th} exponential function. The objectives of Prony's method is to find the weighing value B_i , the eigenvalues λ_i and the order of Prony's expansion n that force the estimated response $\hat{x}(t)$ in Eq. (1) to be least square fit of the signal $x(t)$. Thus, Prony's method can estimate amplitude, frequency and damping ratio of each harmonic component [12, 13].

Forty seconds (approximately 10 times of the natural period of two-loops mode) long piece of record has been selected for all the events, and the harmonic components of each piece of record are identified at every two seconds by moving the starting point of each piece of records every two seconds. The analysis is started at $t = 20(\text{sec})$ such that transient response signal due to the application of the highpass filter can be avoided. It is to be noted that sampling frequency of data, which is very much related to the order of Prony's expansion [13], is selected as 2.5 Hz. The order of Prony's expansion for the specified data set is determined to be 22 by trial and error such that the error of estimation defined in Eq. (2) is limited to be less than 10% for the most of the cases.

$$error = \frac{\|x(t) - \hat{x}(t)\|}{\|x(t)\|} \times 100\% \quad (2)$$

where $\|\bullet\|$ is Root Mean Square (RMS) value. Out of many harmonic components estimated by Prony's method, physically meaningful harmonic components are separated with conditions that RMS ratio defined by Eq. (3), that is contribution of i^{th} harmonic component to the total signal, is greater than 40% and damping ratio is in the range of ± 0.1 .

$$RMS_{ratio}(i) = \frac{\|B_i e^{\lambda_i t}\|}{\|\hat{x}(t)\|} \times 100\%$$

(3)

The results of Prony's analysis, that is, the frequency, damping ratio and amplitude of physically meaningful harmonic components in vertical response at quarter span in Events 1, 2 and 3 are shown in Figs. 6 - 8. All the results of Prony's analysis are indicated by dots (\circ), while dominant harmonic component with maximum amplitude at each time is illustrated by filled dot (\bullet). Fig. 6 depicts the change in frequency composition of meaningful harmonic components in the vertical response of Events 1, 2 and 3 with respect to time. There exists dominant harmonic components with almost constant frequency in Event 1 and with fairly constant frequency in Event 2 with respect to time, as shown in Figs. 6 (a) and (b). The frequency is close to the natural frequency (0.27~0.29 Hz) of the in-plane, 2-loops mode in Phase C. Thus correlated dominant harmonic component with time represents the major galloping component in the vertical response of the respective events. However, there is not the existence of dominant harmonic component with unique frequency correlated with time in the vertical response of Event 3. Many numbers of harmonic components are grouped together in different frequencies level around the single-loop per span frequency of Phase B at different instances, as shown in Fig. 6 (c). It should be noted that the same nature of frequency composition of harmonic components was observed in the horizontal responses of Events 2 and 3. Therefore, the higher frequency responses in both directions of Event 3 and in the horizontal direction of Event 2 can be regarded as random gust response.

As the correlated dominant harmonic component represents the major galloping component of the events, the amplitude and damping ratio of major galloping component of Events 1 and 2 at quarter span can be estimated from Figs. 7 and 8, respectively. Fig. 7 suggests that the amplitude of the major galloping component of Event 1 is higher than that of Event 2 even though the mean wind speed during Event 2 is much higher than in Event 1 as shown in Fig. 3 (d). The damping ratio of major galloping component of both Events 1 and 2 ranges from negative to positive, as shown in Fig. 8, suggesting the fact that the amplitude grows and diminishes with respect to time. The small range of damping ratio in Event 1 shown in Fig. 8 (a) suggests that the amplitude of major galloping component vary gradually with time, while rapid change in the amplitude of major galloping component in Event 2 can be expected on account of high positive as well as negative damping ratio as shown in Fig. 8 (b).

Oscillation orbit and mode of vibration in Event 2

With the results of spectral and Prony's analyses, Events 1 and 3 have been identified as galloping and gust response, respectively. On the contrary, Event 2 contains both galloping and gust response components. Since the galloping frequency has been identified as the in-plane two-loops frequency in Prony's analysis, it is possible to separate major galloping and major gust response components by applying filtering technique. The highpass and lowpass filters with the cut-off frequency of approximately

10% lesser than the identified galloping frequency are, therefore, applied to the response records of Event 2.

Fig. 9 depicts the Lissajous diagrams of major galloping component of Event 2 obtained by applying the highpass filter. The Lissajous diagrams at quarter span and mid span in the figure suggest that the major galloping component is principally vertical motion with the in-plane two-loops mode of vibration. The amplitude of major galloping component in vertical motion at quarter span, shown in Fig. 9, is nearly ± 0.9 meter which is in good agreement with the maximum amplitude estimated by Prony's analysis as shown in Fig. 7 (b).

Obliquely oriented Lissajous diagrams of major gust response of Event 2, obtained by the application of lowpass filter at both quarter and mid spans, can be seen in Fig. 10. Comparable amplitudes of responses in both vertical and horizontal motions with very low frequency reflect the fact that the mode of vibration is swinging type caused by the quasi-static effect of gusty wind. The amplitude of gust response at mid span is significantly large and approximately ranged in ± 1 m in the vertical direction and in ± 1.5 m in the horizontal direction. Since the contribution of major galloping component at mid span is negligibly small because of two-loops mode, the total response at this location is constituted only by the gust response.

Random decrement method for identifying galloping component

Random Decrement method (RDM) [14, 15], which is a method of extracting a non-forced vibration component from random vibration record for damping identification, is also applied to the higher frequency response components of all the events in order to estimate non-forced galloping component.

Non-forced vibration response component extracted by RDM in the vertical response of Events 1, 2 and 3 are shown in Fig. 11. An existence of correlated response component is clearly seen in Event 1 as shown in Fig. 11 (a), which is the evidence of galloping event. The non-forced vibration of Event 2 shown in Fig 11 (b), on the contrary, indicates the existence of trace of correlated response component but not the evidence of a galloping. Furthermore, the non-forced vibration component of Event 3 is still random. The principle of RDM suggests that in the case of stationary Gaussian random excitation, the output of RDM should be free decay response not only with structural damping but also with aerodynamic damping. It has been pointed out from the wind tunnel experiment on 3D model of transmission line [7] that the aerodynamic damping in stable vibration can be varied with time and could reach up to 60% of critical damping ratio in high turbulent wind. Such a large aerodynamic damping in stable transmission line vibration could result the non-forced vibration component of response as shown in Fig. 11 (c) unlike usual free decay response extracted by RDM. Furthermore, it is to be noted that sufficiently large number of random signature to cancel out the random component of response is not available in this problem as is usual in RDM practice to determine free decay response.

Conclusions

A method of identifying different wind-induced vibrations of ice-accreted transmission lines from measured response records is proposed in this study. Applications of well-established spectral analysis and Prony's method have been shown in the problem of identifying dynamic parameters of wind-induced vibration. Possibility of applying RDM to identify general categories of vibration is also discussed. General category of vibration, amplitude, frequency and negative damping ratio in case of galloping event are identified for three typical events of wind-induced vibration under consideration. Besides galloping, occurrence of large amplitude gust response not only in the horizontal direction but also in the vertical direction can be observed. Possibility of separating galloping response component from other categories of response in mixed mode of vibration is highlighted and it is well documented that thus separated response can characterize the galloping event. In case of dead span, the galloping mode is found to be the two-loops mode for the observed typical galloping events. Thus proposed method can be applied to huge numbers of field observed wind-induced vibration of ice-accreted transmission line to characterize galloping as well as gust response.

References

1. Pasha M.A. How to tame galloping of transmission conductors. *Electric World* 1989; 203(7): 43-46.
2. Wang J., Lilien J.L. Overhead electrical transmission line galloping: A full multi-span 3-DOF model, some applications and design recommendations. *IEEE Transactions on Power Delivery* 1998; 13(3): 909-916.
3. Keutgen R., Lilien J.L. Benchmark cases for galloping with results obtained from wind tunnel facilities-validation of a finite element model. *IEEE Transactions on Power Delivery* 2000;15(1): 367-374.
4. Keutgen R. Galloping phenomena a finite element approach. Ph.D. Thesis 1998; University of Liege, Belgium.
5. Yukino T., Fujii K., Hayase I. Galloping Phenomena of large bundle conductors observed on the full scale test line. *Proceeding of International Seminar on Cable Dynamics* 1995; Liege, Belgium: 557-563.
6. Rawlins C.B. Analysis of conductors galloping field observations-single conductors. *IEEE Transactions on Power Apparatus and System* 1981; 100(8): 80-89.
7. Loredou-Souza A.M., Davenport A.G. The effects of high winds on transmission lines. *Journal of Wind Engineering and Industrial Aerodynamics* 1998; 74(76): 987-994.
8. Yamaguchi H., Xie X., Yukino T. Galloping analysis of transmission lines with bundle conductors. *Proceeding of International Seminar on Cable Dynamics* 1995; Liege, Belgium: 61-66.
9. Desai Y.M., Yu P., Popplewell N., Shah A.H. Finite element modeling of transmission line galloping. *Computers and structures* 1995; 57(3): 407-420.
10. Ohkuma T., Marukawa H. Galloping of overhead transmission lines in gusty wind. *First International Conference on Advances in Structural Engineering and Mechanics* 1999; Seoul, Korea: 71-76.
11. Tunstall M.J. Wind induced vibration of overhead transmission lines: an overview. *Proceedings of International Seminar on Cable Dynamics* 1997; Tokyo, Japan:

- 13-35.
12. Pierre D.A., Smith J.R., Trudnowski D.J., and Pierre J.W. Prony based methods for simultaneous identification of transfer functions and initial conditions. *Computers Elect. Engng.* 1995; 21(2): 89-100.
 13. Hauer J.F., Demeure C.J., Scharf L.L. Initial results in Prony analysis of power system response. *IEEE Transactions on Power Systems* 1990; 5(1): 80-89.
 14. Kareem A., Gurley K. Damping in structures: its evaluation and treatment of uncertainty. *Journal of Wind Engineering and Industrial Aerodynamics* 1996; 59:131-157.
 15. Asmussen J.C. Modal analysis based on the random decrement technique-application to civil engineering structures. Ph.D. Thesis 1997; Aalborg University, Denmark.
 16. MATLAB-Signal Processing toolbox. The MatLab Works, Inc.

List of tables:

Table 1 Geometrical descriptions of Tsuruga Test Line [8]

Table 2 Dynamic characteristics of Tsuruga Test Line [5]

List of Figures:

Fig. 1 Top view of Tsuruga Test Line KEPCO

Fig. 2 Lissajous diagrams of typical events observed in Tsuruga Test Line, KEPCO

Fig. 3 Time series of vertical response at quarter span in typical events and time series of wind velocities

Fig. 4 Power spectra of responses at quarter span in typical events

Fig. 5 Power spectra of wind velocities

Fig. 6 Change in frequency composition of harmonic components in vertical responses at quarter span identified by Prony's method

Fig. 7 Amplitude of harmonic components in vertical response at quarter span with frequency close to dominant frequency

Fig. 8 Damping ratio of harmonic components in vertical response at quarter span with frequency close to dominant frequency

Fig. 9 Lissajous diagrams of major galloping component of Event 2 obtained by highpass filter



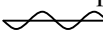

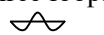


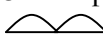

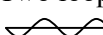
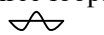
Fig. 10 Lissajous diagrams of major gust response of Event 2 obtained by lowpass filter

Fig. 11 Non-forced vibration component extracted by Random Decrement method

Table 1 Geometrical descriptions of Tsuruga Test Line [8]

Description	Phase B	Phase C
No. of conductors	4	6/8
No. of spans	2	1
Span length (m)	347 x 2	344
Sag to span ratio	0.037	0.042
Unit mass (kg/m/conductor)	3.35	3.35
Axial rigidity (MN/conductor)	65.2	65.2
Conductor diameter (mm)	38.4	30
Conductor spacing (m)	0.50	1.3

Table 2 Dynamic characteristics of Tsuruga Test Line [5]

Motion	Mode of vibration (loop/span)	Phase B	Mode of vibration (loop/span)	Phase C
		Natural frequency (Hz)		Natural frequency (Hz)
Horizontal	One loop 	0.14-0.15	One loop 	0.14
	Two loops 	0.28-0.315	Two loops 	0.281
	---	---	Three loops 	0.422
Vertical	One loop (up-down) 	0.166, 0.284	Quasi-one loop 	0.349-0.469
	One loop (up-up) 	0.288-0.320	Two loops 	0.275-0.315
	Two loops 	0.280-0.312	Three loops 	0.470-0.375
Torsion	One loop	--	One loop	0.125-0.148
	Two loop	0.28-0.386	Two loops	0.225-0.297
			Three loops	0.375-0.444

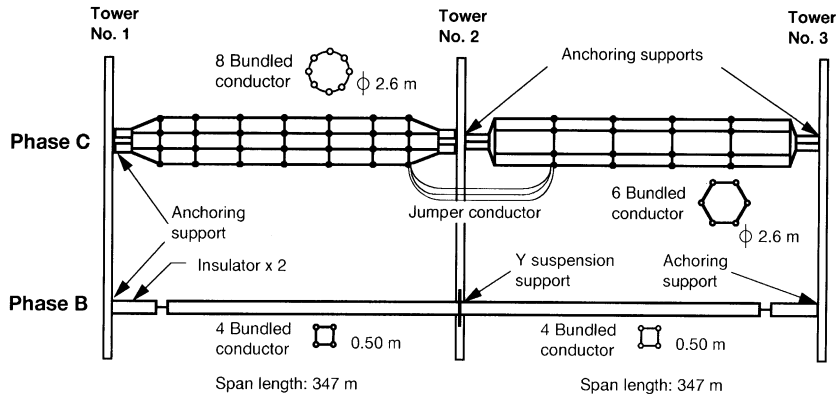
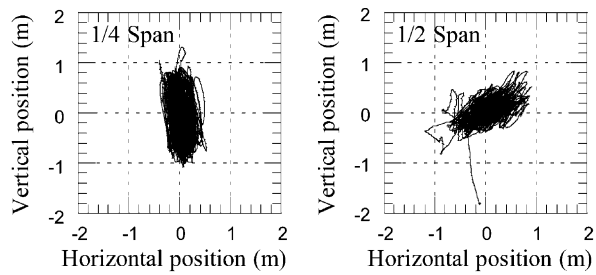
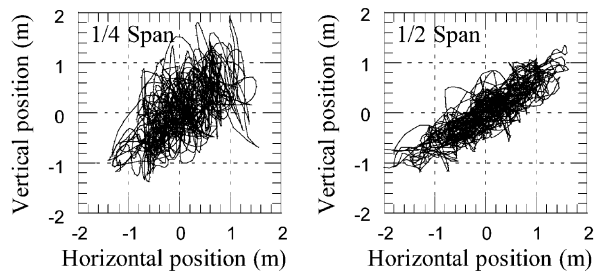


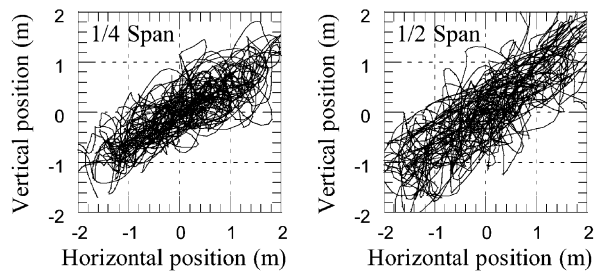
Fig. 1. Top view of the Tsuruga Test Line, KEPCO.



(a) Event 1

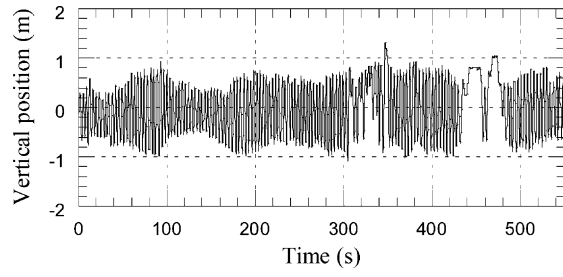


(b) Event 2

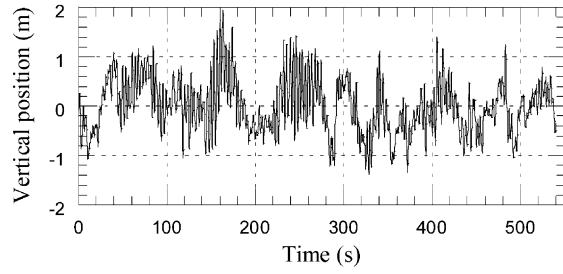


(c) Event 3

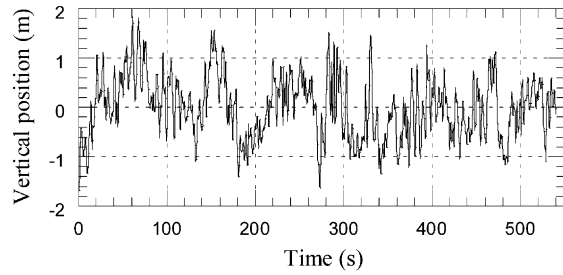
Fig. 2. Lissajous diagrams of typical events observed in the Tsuruga Test Line, KEPCO.



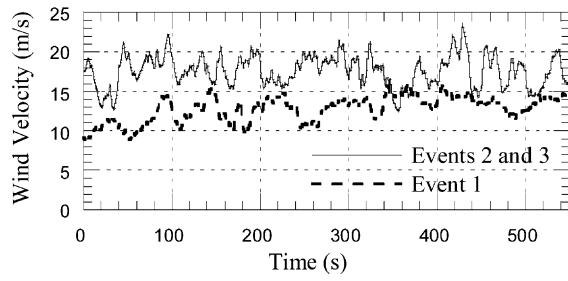
(a) **Event 1**



(b) **Event 2**

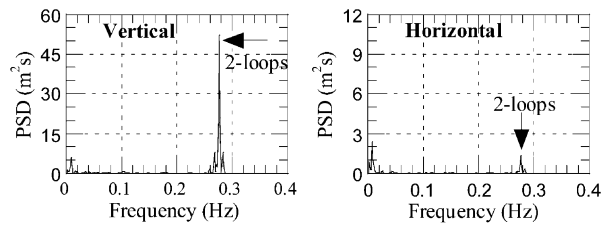


(c) **Event 3**

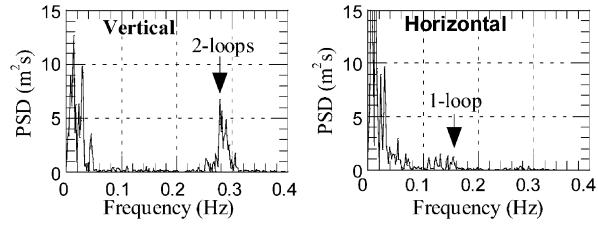


(d) **Wind velocities**

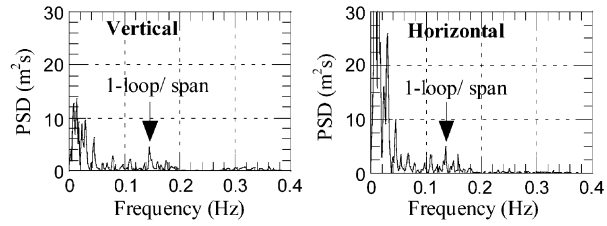
Fig. 3. Time series of vertical responses at quarter span in typical events and time series of wind velocities.



(a) Event 1



(b) Event 2



(c) Event 3

Fig. 4. Power spectra of responses at quarter span in typical events.

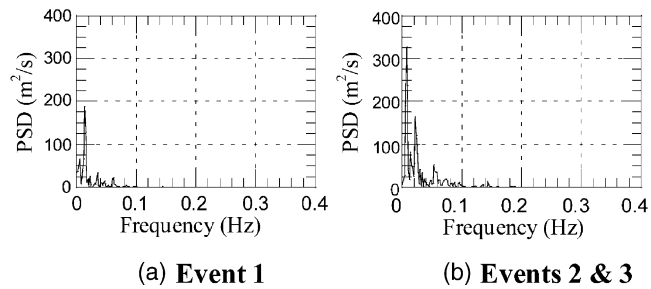
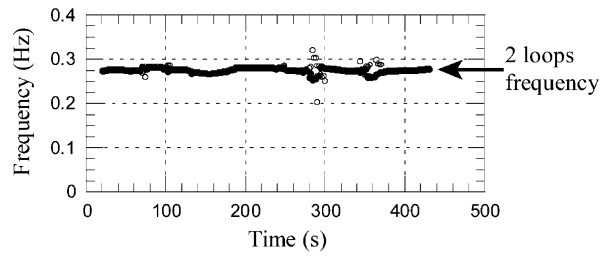
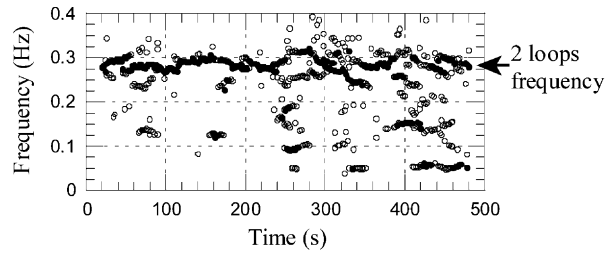


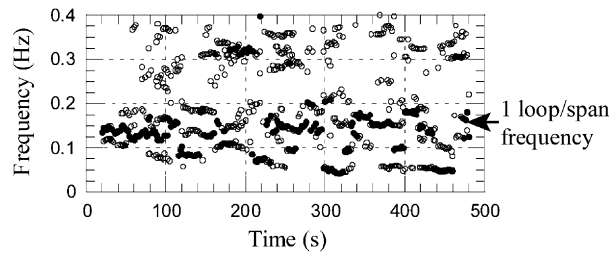
Fig. 5. Power spectra of wind velocities.



(a) Event 1

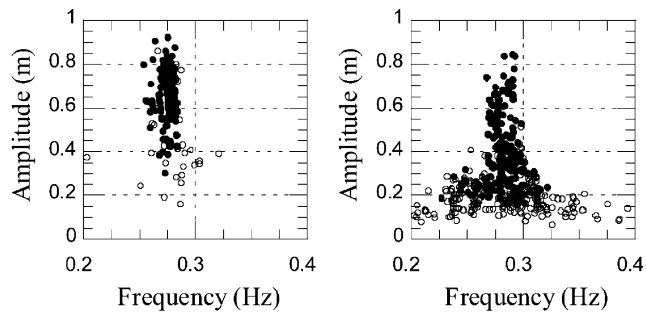


(b) Event 2



(c) Event 3

Fig. 6. Change in frequency composition of harmonic components in the vertical responses at quarter span identified by Prony's method: (●) dominant component.



(a) Event 1

(b) Event 2

Fig. 7. Amplitude of harmonic components in the vertical response at quarter span with frequency close to dominant frequency: (●) dominant component.

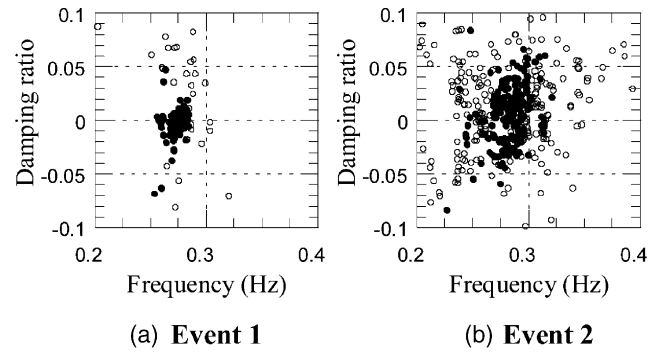


Fig. 8. Damping ratio of harmonic components in the vertical response at quarter span with frequency close to dominant frequency: (●) dominant component.

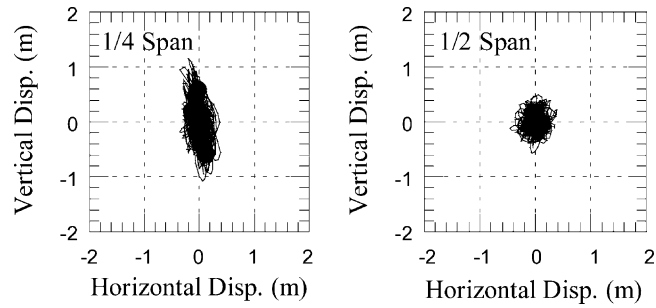


Fig. 9. Lissajous diagrams of the major galloping component in Event 2 obtained by highpass filter.

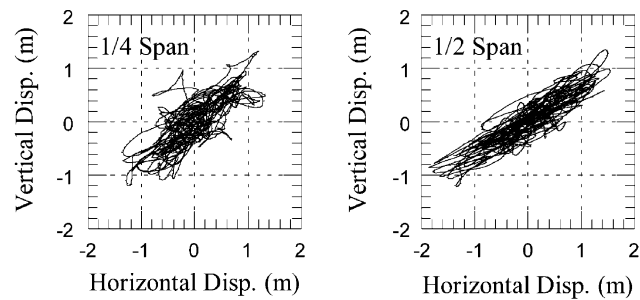
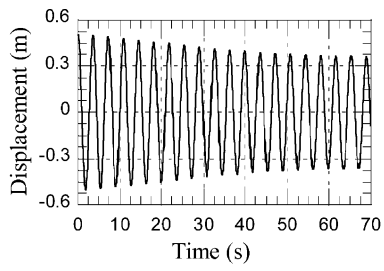
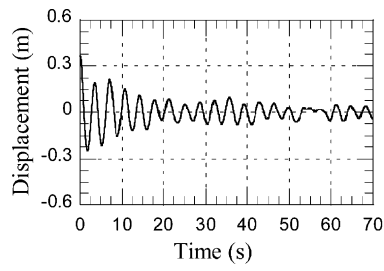


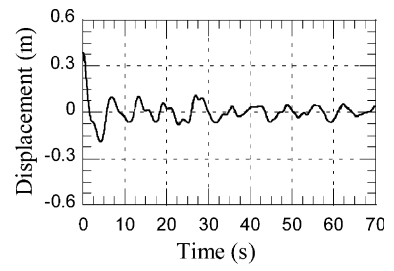
Fig. 10. Lissajous diagrams of the major gust response in Event 2 obtained by lowpass filter.



(a) **Event 1**



(b) **Event 2**



(c) **Event 3**

Fig. 11. Non-forced vibration components extracted by the random decrement method.